JOURNAL OF SOLID STATE CHEMISTRY 6, 419–429 (1973)

Structural Aspects of the Metal–Insulator Transition in V_4O_7

M. MAREZIO, D. B. McWHAN, P. D. DERNIER, AND J. P. REMEIKA

Bell Laboratories, Murray Hill, New Jersey 07974

Received June 19, 1972

V_4O_7 has a transition with decreasing temperature at 250 K and the structure has been refined at 298 and 200 K. The triclinic structure ($A\bar{1}$) consists of rutile-like layers of VO_6 octahedra extending indefinitely in the *a–b* plane and four octahedra thick along the *c*-axis. The average V–O distances for the four independent V atoms are 1.967, 1.980, 1.969, and 1.984 Å at 298K and 1.948, 1.992. 1.961, and 2.009 Å at 200K. At 200K there is a clear separation into strings of V^{3+} or V^{4+} ions running parallel to the pseudorutile *c*-axis. In addition, all of the 3+ and half of the 4+ sites are paired to form short V–V bonds. The remaining V^{4+} atom is displaced toward one oxygen so as to balance its electrostatic charge. The distortion at the metal–insulator transitions in V_4O_7, Ti_4O_7, VO_2 + Cr, and NbO_2 are compared.

Introduction

In a recent letter (*1*) we reported that charge localization occurs at the metal–insulator transitions of Ti_4O_7 and V_4O_7. It was found that in the insulating phases chains of M^{3+} and M^{4+} ions run parallel to the pseudorutile *c*-axis, whereas these ions are disordered in the metallic phases. The charge localization is accompanied by either a bond pairing of adjacent cations or a displacement of the cation toward one of the neighboring oxygen atoms, forming zigzag chains of unpaired cations. In this paper we report the detailed results of the crystal structure refinements of V_4O_7 at room temperature and at 200K. We also compare the metal–insulator transition of V_4O_7 with that of Ti_4O_7, VO_2, VO_2 + Cr, and NbO_2. The detailed results on Ti_4O_7 have been published elsewhere (*2*).

The oxide V_4O_7 is a member of the homologous series V_nO_{2n-1}, which is isostructural with the Ti_nO_{2n-1} series. The triclinic structure of V_4O_7 can be described in space group $A\bar{1}$ with four formulas per unit cell (*3*). The relationship between the triclinic cell and the rutile subcell is given by:

$$\begin{pmatrix}\mathbf{a}_t\\ \mathbf{b}_t\\ \mathbf{c}_t\end{pmatrix} = \begin{pmatrix}\bar{1} & 0 & 1\\ 1 & 1 & 1\\ 1 & \bar{2} & 2\end{pmatrix}\begin{pmatrix}\mathbf{a}_R\\ \mathbf{b}_R\\ \mathbf{c}_R\end{pmatrix}.$$

Horiuchi et al. (*4*) who studied the crystallography of the series V_nO_{2n-1}, proposed a primitive cell related to the A-centered cell by:

$$\begin{pmatrix}\mathbf{a}_t\\ \mathbf{b}_t\\ \mathbf{c}_t\end{pmatrix}_P = \begin{pmatrix}1 & 0 & 0\\ 0 & 1 & 0\\ 2 & 5/2 & 1/2\end{pmatrix}\begin{pmatrix}\mathbf{a}_t\\ \mathbf{b}_t\\ \mathbf{c}_t\end{pmatrix}_A$$

For comparative and descriptive purposes, however, we will adopt the non-standard A-centered cell.

There is only one metal–insulator transition at 250K in V_4O_7 (*5*), while at 40K it undergoes a paramagnetic–antiferromagnetic transition (*6*). At 250K the resistivity increases discontinuously by a factor of 50 and it rises rapidly below the transition and saturates at 10^6 times the metallic value by 120K (*5*). The magnetic susceptibility drops in a similar manner by a factor of 2 (*7*). A very small increase in the unit-cell volume occurs at 250K (*8*). The discontinuities observed in the lattice parameters at the metal–insulator transition in V_4O_7 are different in magnitude and/or in sign from those observed in Ti_4O_7. This indicates that from the crystallographic point of view the nature of the transition in V_4O_7, which has one additional *d* electron per cation, is different from that occurring in Ti_4O_7.

Crystal Data

The crystals of V_4O_7 were grown from a powder sample by the method of vapor transport. The powder sample was made by heating the appro-

priate mixture of V_2O_3 and VO_2 in an evacuated quartz tube at 800°C for 16 hr and then at 1000°C for 5 hr. The crystals were grown as described by Nagasawa using $TeCl_4$ as the transporting agent (*9*). Because commercial $TeCl_4$ contains some TeO_2, which would oxidize the vanadium oxide, the $TeCl_4$ was distilled in a vacuum prior to use.

Figure 1 shows the variation of the lattice parameters as a function of temperature. A clear discontinuity in volume and lattice parameters is seen at the metal–insulator transition at 250K but no anomalies were observed at the Néel temperature (40K). The points represented by circles are from Ref. (*8*). The squares are new values determined by using the V_4O_7 powder prepared as described above. X-ray traces were obtained from a Phillips diffractometer equipped with an Air-Products and Chemicals Cryotip device. The diffractometer zero was determined by using a silicon internal standard. The lattice parameter least-squares refinements were carried out using 24 well-resolved reflections. The previously determined points obtained from different equipment and powder were scaled appropriately.

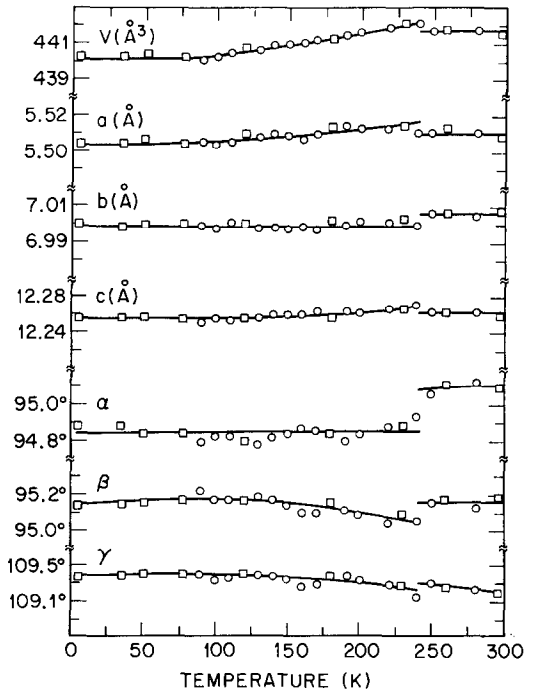

FIG. 1. Lattice parameters and volume vs temperature for V_4O_7. The parameters are given for the A-centered unit cell containing four formulas per cell. The significance of the squares and circles is described in the text.

Single Crystal Intensity Data Collection

The intensity measurements were taken with a paper-tape-controlled automatic GEXRD-5 diffractometer. An 8° takeoff angle was used along with a scintillation counter, decade scalar, and single Zr-filtered Mo$K\alpha$ radiation. The integrated intensities were obtained by use of the stationary crystal–stationary counter technique. The specimen was a sphere of radius $R = 0.013$ cm. which was oriented with the [$\bar{1}$20] zone axis along the ϕ circle axis. At room temperature all reflections in the upper hemisphere with $25° \leqslant 2\theta \leqslant 70°$ were measured with the diffractometer in a fully automatic mode. The background was measured $\pm 2°$ off the peak maximum. A standard reflection ($\bar{1}$04) was measured every hour so as to keep a running check on the crystal orientation. A total of 1883 reflections were measured, of which 1254 were independent and well above background.

At 200K only those reflections well above background at 298K were measured. The temperature was maintained by blowing a cold stream of nitrogen gas directly on the crystal. A Varian control unit was used to minotor and control the proper gas flow. As indicated in Fig. 2 the intensity of the reflection (251) was a very sensitive indicator of the relative temperature and therefore it was used as a standard along with a strong

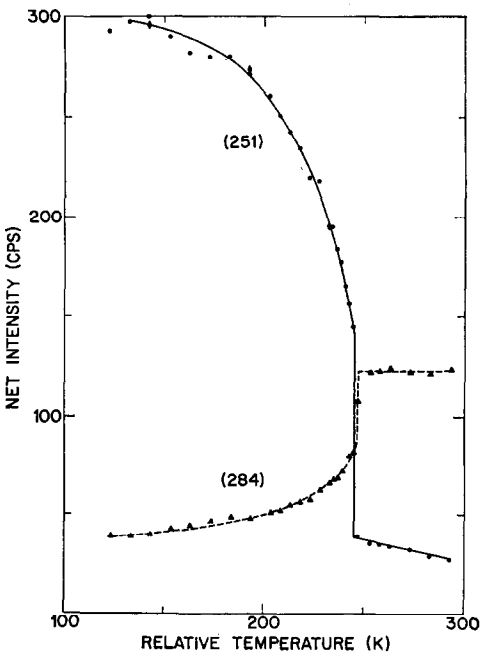

FIG. 2. Net intensities of the reflections (251) and (284) vs relative temperature for the V_4O_7 crystal sphere.

reflection ($\bar{1}04$) as a check of sample orientation and ice buildup. The procedure for collecting intensities was semiautomatic. For each reflection the approximate angles 2θ, χ, and ϕ were set automatically and then maximized by hand. The total number of observed reflections was 851. The Lorentz, polarization, and absorption corrections were applied in order to convert the integrated intensities into structure factors. The absorption coefficient for Mo$K\alpha$ was taken as 86.7 cm^{-1}, with $\mu R = 1.11$. All Friedel pairs corresponding to weak reflections were measured by hand at both temperatures and within experimental limits no differences between (hkl) and ($h\bar{k}l$) were observed. This strongly indicated that the correct space group was $A\bar{1}$ for both structures.

TABLE I

FINAL POSITIONAL PARAMETERS

	298K	200K
V(1)x	0.21437(7)	0.20403(8)
y	0.14740(5)	0.14097(7)
z	0.06317(3)	0.06209(4)
V(2)x	0.22314(7)	0.23447(8)
y	0.65454(5)	0.65444(7)
z	0.06686(3)	0.06923(4)
V(3)x	0.68224(6)	0.68560(7)
y	0.44016(5)	0.44065(6)
z	0.19969(3)	0.19798(4)
V(4)x	0.68734(6)	0.68157(7)
y	0.94206(5)	0.94085(7)
z	0.20173(3)	0.20017(4)
O(1)x	0.1014(3)	0.1055(3)
y	0.8576(2)	0.8543(3)
z	0.0150(1)	0.0138(2)
O(2)x	0.5852(3)	0.5920(3)
y	0.7954(2)	0.7932(3)
z	0.0542(1)	0.0472(2)
O(3)x	0.8547(3)	0.8571(3)
y	0.4937(2)	0.4942(3)
z	0.0835(1)	0.0860(2)
O(4)x	0.3265(3)	0.3305(3)
y	0.4356(2)	0.4347(3)
z	0.1374(1)	0.1373(2)
O(5)x	0.5257(3)	0.5247(3)
y	0.1437(2)	0.1449(3)
z	0.1643(1)	0.1643(2)
O(6)x	0.0309(3)	0.0418(3)
y	0.0639(2)	0.0662(3)
z	0.1977(1)	0.1948(2)
O(7)x	0.2953(3)	0.2955(3)
y	0.7921(2)	0.7925(3)
z	0.2245(1)	0.2250(2)

Refinements

Least-squares refinements were carried out by using the program written by C. T. Prewitt (*10*). The starting positional and thermal parameters for the 298K refinement were those of Ti_4O_7 (*2*). The form factor tables for neutral atoms given by Cromer and Waber (*11*) were used together with the values of $\Delta f'$ and $\Delta f''$ for vanadium reported by Cromer (*12*). The function minimized was $\sum w||F_o| - |F_c||^2$, where $w = 1/\sigma^2$, $\sigma = 1.5$ when $|F_o| \leq 15$ and $\sigma = 0.1|F_o|$ when $|F_o| > 15$. In the first cycles the scale factor, the secondary extinction coefficient, 33 positional parameters and 11 isotropic thermal parameters were varied. The conventional R and wR factors were 0.042 and 0.062, respectively. In the last four cycles anisotropic thermal parameters were introduced. This resulted in $R = 0.029$ and $wR = 0.045$, indicating that the thermal anisotropy was appreciable. The refinements of the low temperature data were performed following the same procedure. The R and wR factors corresponding to the isotropic refinements were 0.031 and 0.047, respectively. They decreased to 0.023 and 0.038 after the introduction of anisotropic thermal parameters. The final positional and thermal parameters for the two temperatures are reported in Tables I and II. These values together with the lattice parameters as listed below were input to the program ORFFE (*13*), which gave the

TABLE II

FINAL THERMAL PARAMETERS ($\times 10^4$)

	298K	200K
V(1)β_{11}	30(1)	26(1)
β_{22}	23.9(9)	16(1)
β_{33}	6.6(2)	4.8(3)
β_{12}	15.0(8)	5.8(8)
β_{13}	−1.9(4)	0.4(4)
β_{23}	−0.8(4)	1.9(5)
V(2)β_{11}	29(1)	24(1)
β_{22}	23.9(9)	14(1)
β_{33}	6.3(3)	5.3(3)
β_{12}	14.2(8)	3.7(8)
β_{13}	0.6(4)	1.9(4)
β_{23}	0.1(4)	2.4(5)

TABLE II—*continued*

	298K	200K
V(3)β_{11}	25(1)	19(1)
β_{22}	22.1(8)	15(1)
β_{33}	6.3(2)	4.4(3)
β_{12}	12.4(7)	2.9(8)
β_{13}	2.2(4)	2.1(4)
β_{23}	−0.9(3)	2.1(4)
V(4)β_{11}	28(1)	23(1)
β_{22}	25.3(8)	15(1)
β_{33}	6.9(2)	6.3(3)
β_{12}	17.8(7)	6.7(8)
β_{13}	3.1(4)	4.0(4)
β_{23}	1.0(3)	3.9(5)
O(1)β_{11}	39(4)	28(5)
β_{22}	25(3)	17(3)
β_{33}	10.8(8)	8(1)
β_{12}	19(3)	8(3)
β_{13}	−2(1)	−1(2)
β_{23}	0(1)	2(2)
O(2)β_{11}	29(4)	39(5)
β_{22}	35(3)	25(4)
β_{33}	8.4(8)	8(1)
β_{12}	9(3)	11(3)
β_{13}	1(1)	0(2)
β_{23}	0(1)	2(2)
O(3)β_{11}	41(4)	33(5)
β_{22}	33(3)	26(4)
β_{33}	8.2(7)	6(1)
β_{12}	15(3)	5(3)
β_{13}	5(1)	1(2)
β_{23}	2(1)	4(2)
O(4)β_{11}	48(4)	32(5)
β_{22}	31(3)	19(3)
β_{33}	5.7(7)	9(1)
β_{12}	22(3)	5(3)
β_{13}	0(1)	1(2)
β_{23}	1(1)	0(2)
O(5)β_{11}	33(4)	34(5)
β_{22}	23(2)	13(3)
β_{33}	6.3(7)	8(1)
β_{12}	14(2)	4(3)
β_{13}	−1(1)	2(2)
β_{23}	0(1)	2(2)
O(6)β_{11}	30(4)	25(4)
β_{22}	32(3)	29(4)
β_{33}	10.7(8)	8(1)
β_{12}	15(3)	7(3)
β_{13}	−1(1)	0(2)
β_{23}	0(1)	2(2)
O(7)β_{11}	34(4)	37(5)
β_{22}	28(3)	16(3)
β_{33}	6.5(7)	7(1)
β_{12}	18(3)	10(3)
β_{13}	−1(1)	−2(2)
β_{23}	1(1)	2(2)

interatomic distances, and thermal data reported in Tables III–VI.[1]

	298K	200K
a =	5.509(1) Å	5.514(2) Å
b =	7.008(1)	7.004(2)
c =	12.258(2)	12.260(4)
α =	95.09(1)°	94.86(1)°
β =	95.19(1)	95.14(1)
γ =	109.21(1)	109.30(1).

Description of the Structure

The structure of V_4O_7 consists of a distorted hexagonal close-packed oxygen array. The

TABLE III

INTERATOMIC DISTANCES (Å) IN V-OCTAHEDRA[a]

	298K	200K
V(1)–O(1)	1.897	1.881
–O(1)	1.937	1.923
–O(2)	1.883	1.818
–O(4)	2.010	2.046
–O(5)	2.032	2.065
–O(6)	2.042	1.954
Average	1.967	1.948
O(5)–O(6)	2.674	2.603
O(5)–O(4)	2.651	2.620
O(5)–O(2)	2.793	2.720
O(5)–O(1)	2.885	2.895
O(1)–O(6)	2.795	2.772
O(1)–O(4)	2.933	2.943
O(1)–O(2)	2.824	2.794
O(1)–O(1)	2.625	2.693
O(2)–O(4)	2.902	2.804
O(2)–O(1)	2.736	2.692
O(6)–O(4)	2,784	2.736
O(6)–O(1)	2.685	2.679
V(2)–O(1)	1.895	1.913
–O(2)	1.940	1.944
–O(3)	2.010	2.051
–O(3)	1.970	2.027
–O(4)	2.037	2.005
–O(7)	2.025	2.013
Average	1.980	1.992

[1] A table of observed and calculated structure factors has been deposited as Document No. NAPS-01815 with the ASIS National Auxiliary Publications Service, C/O CCM Information Corp., 909 Third Avenue, New York, 10022. A copy may be secured by citing the document number and by remitting the price for photocopies or microfiche. Advance payment is required. Make check or money order payable to ASIS-NAPS. (For current prices please check with NAPS.)

TABLE III—*continued*

	298K	200K
O(7)–O(1)	2.826	2.827
O(7)–O(2)	2.739	2.839
O(7)–O(3)	2.918	2.904
O(7)–O(4)	2.694	2.715
O(3)–O(1)	2.737	2.715
O(3)–O(2)	2.872	2.877
O(3)–O(3)	2.700	2.735
O(3)–O(4)	2.941	2.980
O(3)–O(1)	2.713	2.708
O(3)–O(4)	2.791	2.802
O(2)–O(1)	2.845	2.852
O(2)–O(4)	2.790	2.823
V(3)–O(5)	2.125	2.149
–O(6)	1.938	1.922
–O(7)	1.979	1.988
–O(5)	1.960	1.956
–O(4)	2.027	2.017
–O(3)	1.783	1.733
Average	1.969	1.961
O(6)–O(5)	2.674	2.603
O(6)–O(7)	2.776	2.751
O(6)–O(5)	2.893	2.875
O(6)–O(3)	2.794	2.791
O(4)–O(5)	2.657	2.653
O(4)–O(7)	2.649	2.642
O(4)–O(5)	2.651	2.620
O(4)–O(3)	2.947	2.928
O(5)–O(7)	2.581	2.581
O(5)–O(5)	2.559	2.550
O(3)–O(7)	3.003	2.983
O(3)–O(5)	2.849	2.831
V(4)–O(4)	2.098	2.122
–O(2)	1.937	2.000
–O(7)	1.967	1.974
–O(7)	2.125	2.100
–O(6)	1.810	1.898
–O(5)	1.967	1.959
Average	1.984	2.009
O(4)–O(7)	2.694	2.715
O(4)–O(7)	2.649	2.642
O(4)–O(6)	2.947	3.034
O(4)–O(5)	2.657	2.653
O(2)–O(7)	2.899	2.961
O(2)–O(7)	2.739	2.839
O(2)–O(6)	2.874	2.926
O(2)–O(5)	2.812	2.892
O(7)–O(7)	2.552	2.552
O(7)–O(5)	2.581	2.581
O(6)–O(7)	2.853	2.897
O(6)–O(5)	3.015	3.075

[a] The standard deviations for all interatomic distances in this table are ± 0.002 Å except for the 200K O–O distances where it is ± 0.003 Å.

TABLE IV

V–V DISTANCES (Å)[a]

	298K	200K
V(1)–V(1) edge[b]	2.794	2.687
–V(3) edge[b]	2.964	3.027
–V(2) corner[b]	3.539	3.547
–V(2) corner[b]	3.489	3.532
–V(2) corner[a]	3.474	3.475
–V(2) corner[b]	3.535	3.538
–V(4) corner[b]	3.721	3.716
–V(4) corner[b]	3.459	3.426
–V(4) corner[b]	3.378	3.370
–V(3) edge[c]	3.066	3.089
–V(4) corner[c]	3.755	3.805
V(2)–V(2) edge[b]	2.926	3.024
–V(4) edge[b]	2.930	2.856
–V(1) corner[b]	3.539	3.547
–V(1) corner[b]	3.489	3.532
–V(1) corner[b]	3.474	3.475
–V(1) corner[b]	3.535	3.538
–V(3) corner[b]	3.673	3.617
–V(3) corner[b]	3.486	3.486
–V(3) corner[b]	3.397	3.384
–V(4) edge[c]	3.009	2.990
–V(3) corner[c]	3.720	3.737
V(3)–V(1) edge[b]	2.964	3.027
–V(2) corner[b]	3.673	3.617
–V(2) corner[b]	3.486	3.486
–V(2) corner[b]	3.397	3.384
–V(4) corner[b]	3.502	3.496
–V(4) corner[b]	3.506	3.509
–V(4) face[c]	2.768	2.781
–V(4) corner[c]	3.374	3.399
–V(3) edge[c]	3.189	3.222
–V(1) edge[c]	3.066	3.089
–V(2) corner[c]	3.720	3.737
V(4)–V(2) edge[b]	2.930	2.856
–V(1) corner[b]	3.721	3.716
–V(1) corner[b]	3.459	3.426
–V(1) corner[b]	3.378	3.370
–V(3) corner[b]	3,502	3.496
–V(3) corner[b]	3.506	3.509
–V(3) face[c]	2.768	2.781
–V(3) corner[c]	3.374	3.399
–V(4) edge[c]	3.202	3.178
–V(2) edge[c]	3.009	2.990
–V(1) corner[c]	3.755	3.805

[a] The standard deviations for all distances in this table are ± 0.001 Å.
[b] Distances inside the rutile blocks.
[c] Distances between rutile blocks.

vanadium atoms occupy the octahedral sites so as to form rutile blocks which extend indefinitely in the triclinic *a–b* plane and are four octahedra thick along the perpendicular to this plane.

TABLE V

ROOT MEAN SQUARE VALUES

	298K	200K
V(1)r_1	0.053(2)	0.056(3)
r_2	0.065(2)	0.058(2)
r_3	0.083(1)	0.066(1)
V(2)r_2	0.055(2)	0.051(3)
r_2	0.066(1)	0.061(2)
r_3	0.077(1)	0.065(1)
V(3)r_1	0.049(2)	0.047(3)
r_2	0.065(1)	0.057(2)
r_3	0.076(1)	0.062(1)
V(4)r_1	0.046(2)	0.049(3)
r_2	0.072(1)	0.055(2)
r_3	0.078(1)	0.072(1)
O(1)r_1	0.055(5)	0.056(7)
r_2	0.076(3)	0.062(6)
r_3	0.096(3)	0.082(4)
O(2)r_1	0.062(4)	0.068(6)
r_2	0.078(4)	0.073(5)
r_3	0.091(4)	0.083(4)
O(3)r_1	0.069(4)	0.061(11)
r_2	0.080(4)	0.065(5)
r_3	0.085(4)	0.084(4)
O(4)r_1	0.062(5)	0.061(5)
r_2	0.068(4)	0.070(4)
r_3	0.089(3)	0.082(7)
O(5)r_1	0.058(5)	0.053(8)
r_2	0.066(4)	0.071(4)
r_3	0.078(4)	0.076(5)
O(6)r_1	0.059(5)	0.057(5)
r_2	0.081(3)	0.077(7)
r_3	0.095(4)	0.081(4)
O(7)r_1	0.055(5)	0.052(10)
r_2	0.070(4)	0.066(5)
r_3	0.083(4)	0.081(4)

Figure 3 is a projection of the structure down the triclinic a-axis. The pseudorutile c-axis runs roughly parallel to the shaded set of octahedra. Between rutile blocks the octahedra-containing cations share faces, whereas in pure rutile there is only edge and corner sharing. The planes containing the shared octahedral faces are called crystallographic shear planes and they are parallel to the triclinic a–b plane.

There are four crystallographically independent cations, V(1) and V(2) inside the rutile blocks and V(3) and V(4) at the end of the blocks. At room temperature the average V–O distances are: V(1)–O = 1.967 Å, V(2)–O = 1.980 Å, V(3)–O = 1.969 Å, and V(4)–O = 1.984 Å. From the ionic radii for 3- and 4-coordinated O^{2-} and 6-coordinated V^{3+} and V^{4+}, one obtains 1.97Å for $V^{3.5+}$–O distance (*14*),[1] which compares very well with the overall average of 1.975 Å. The V–O distances are clearly larger for the V(2) and V(4) octahedra, which indicate that the V(4)–V(2)–V(2)–V(4) chains contain more V^{3+} cations than the V(3)–V(1)–V(1)–V(3) chains. This is somewhat different from the charge distribution found in Ti_4O_7 at room temperature, where the formal charges are almost completely disordered (*2*). Inside a rutile block the shortest V–V distances are across the shared octahedral edges. In the 4–2–2–4 chains the vanadium atoms are nearly equally spaced, whereas in the 3–1–1–3 chains the V(1)–V(1) separation is significantly shorter than the V(1)–V(3) one. Also this pattern of the V–V distances is different from that of Ti_4O_7 (*2*). The V–V average distance across shared octahedral edges inside a rutile block is 2.918 Å. Its counterpart in pure VO_2 is 2.895 Å at 298K (*15*). The shortest V–V distance between blocks is 2.786 Å across the shared octahedral face. Between blocks the V–V distances across the shared octahedral edges vary between 3.009 and 3.203 Å. In metallic V_2O_3 (*16*) the equivalent V–V distances are 2.697 and 2.882 Å across the shared octahedral face and the shared octahedral

TABLE VI

	298K	200K
Root mean square components in the direction of the pseudorutile c-axis		
V(1)	0.064(1)	0.058(2)
V(2)	0.067(1)	0.059(2)
V(3)	0.065(1)	0.054(2)
V(4)	0.073(1)	0.066(1)
Root mean square components in the direction of the pseudorutile [110]		
V(1)	0.077(1)	0.057(3)
V(2)	0.074(1)	0.055(4)
V(3)	0.076(1)	0.053(4)
V(4)	0.075(1)	0.053(3)
Root mean square components in the direction of the V(3)–V(4) vector		
V(3)	0.050(2)	0.057(2)
V(4)	0.049(2)	0.057(2)

[1] A slightly lower value for the V^{4+} ionic radius is assumed than that quoted in Ref. (*14*). This new value is based on recent refinements of the structures of VO_2 (*15*) and $V_{0.976}Cr_{0.024}O_2$ (*18*).

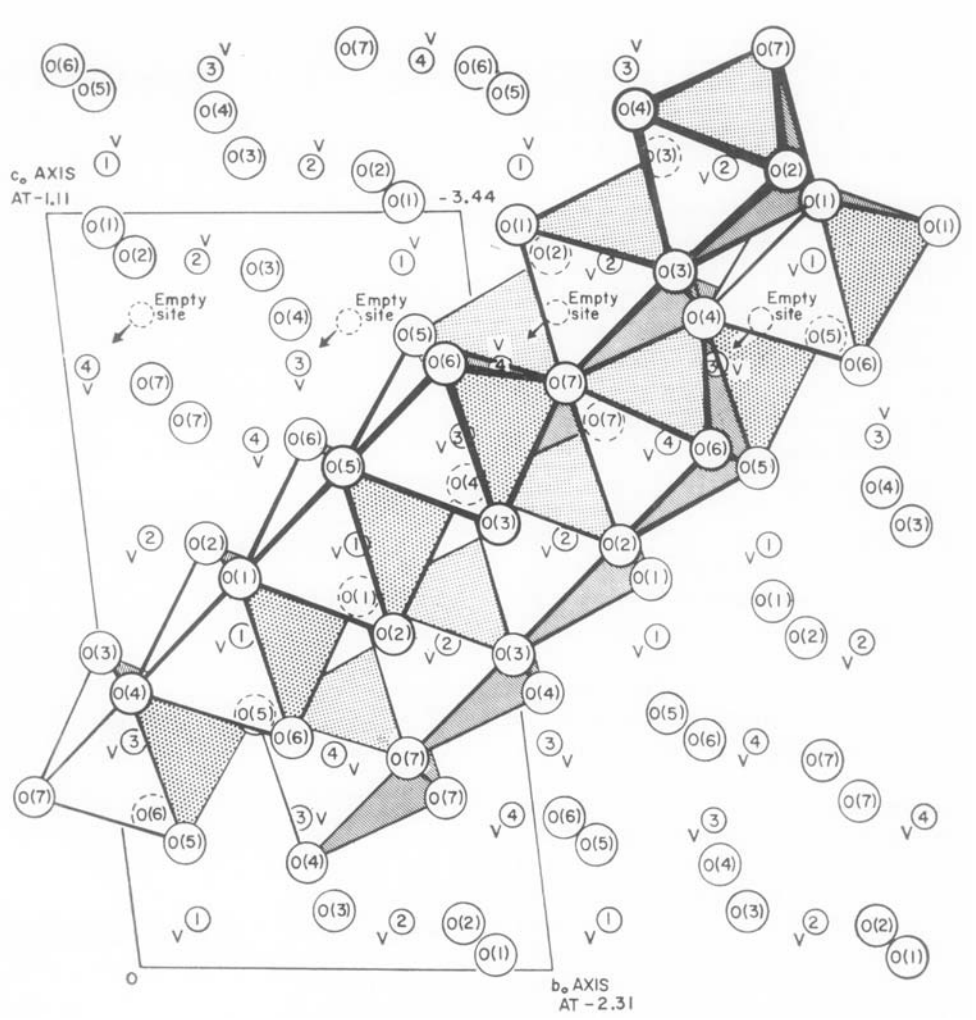

FIG. 3. A projection of the V_4O_7 structure down the triclinic *a*-axis. The *b*–*c* plane slopes down and away from the origin. The shaded set of octahedra runs roughly parallel with the pseudorutile *c*-axis.

edge, respectively. Therefore, the cation bonding across the corundum-like layers in V_4O_7 is substantially weaker than in the corundum structure of V_2O_3.

At 200K for the individual octahedra the average V–O distances are: V(1)–O = 1.948 Å, V(2)–O = 1.992 Å, V(3)–O = 1.961 Å, and V(4)–O = 2.009 Å, the overall average being 1.977 Å. The predicted values for V^{3+}–O and V^{4+}–O are 2.01 and 1.94 Å, respectively (*14*, *15*). The ordering of the V^{3+} and V^{4+} ions is now complete for the V(1) and V(4) sites, whereas some residual disorder occurs at the V(2) and V(3) sites. As the intensities shown in Fig. 2 are still markedly varying with temperature at 200K, the charge localization may increase further at lower temperatures.

Along the chains V(3)–V(1)–V(1)–V(3) the shortest distance, V(1)–V(1), decreases further from 2.794 at 298K to 2.687 Å at 200K, whereas the longer V(3)–V(1) distance of 2.964 Å expands to 3.027 Å. By contrast the shortest V(2)–V(2) distance of 2.926 Å at 298K along the 4–2–2–4 chain expands to 3.024 Å; while the two longer V(4)–V(2) distances of 2.930 Å decrease to 2.856 Å at 200K. Thus there are effectively two short V–V bonds along the 4–2–2–4 chains of cations with formal charge 3+, while only one V–V bond along the 3–1–1–3 chains with cations of formal charge 4+. This pairing pattern is different from that observed in Ti_4O_7, where the cations of the chains 3–1–1–3 become 3+ and form two paired bonds, while the cations of the chains 4–2–2–4 become 4+ and remain unpaired

(*2*). A common feature of the structures of V_4O_7 and Ti_4O_7 in the insulating state is that in both structures there is no pairing across the shared octahedral face. In V_4O_7 this V–V distance increases from 2.768 Å at 298K to 2.781 Å at 200K.

At 298K the V(3) and V(4) octahedra are more distorted than the V(1) and V(2) ones. This is due to face sharing between the V(3) and V(4) octahedra at the end of the rutile blocks. The data at 200K indicate that at the metal–insulator transition the distortion of the V(1) and V(3) octahedra increases, whereas that of the V(2) and V(4) octahedra decreases. A similar effect occurs in Ti_4O_7 where the distortion of the octahedra around the paired cations, Ti(1) and Ti(3), decreases while the distortion of the octahedra around the unpaired cations, Ti(2) and Ti(4), increases. This indicates that in the metallic state the distortion of the octahedra is influenced by the face-sharing while in the insulating state the distortion is influenced predominantly by the cation bonding. Finally one should note that only the unpaired V(3) cation moves out of the center of the octahedron predominantly toward an oxygen.

The root-mean-square components of the thermal displacement are given in Tables V and VI. It can be seen that the thermal vibration of both cations and anions is anisotropic at 298 and 200K. By contrast less anisotropy was observed in Ti_4O_7 at 298K, but more below the transition. It can be seen from the values reported in Tables V and VI that the principal axes of the vanadium thermal ellipsoids are not preferentially aligned with the pseudorutile axes.

Discussion

The distortions found at low temperature in V_4O_7 and Ti_4O_7 can be compared with those found in VO_2 (*15*, *17*), $V_{0.976}Cr_{0.024}O_2$ (*18*), and NbO_2 (*19*). In all cases some of the metal atoms pair to form alternate long and short metal–metal distances along the pseudorutile *c*-axis. In

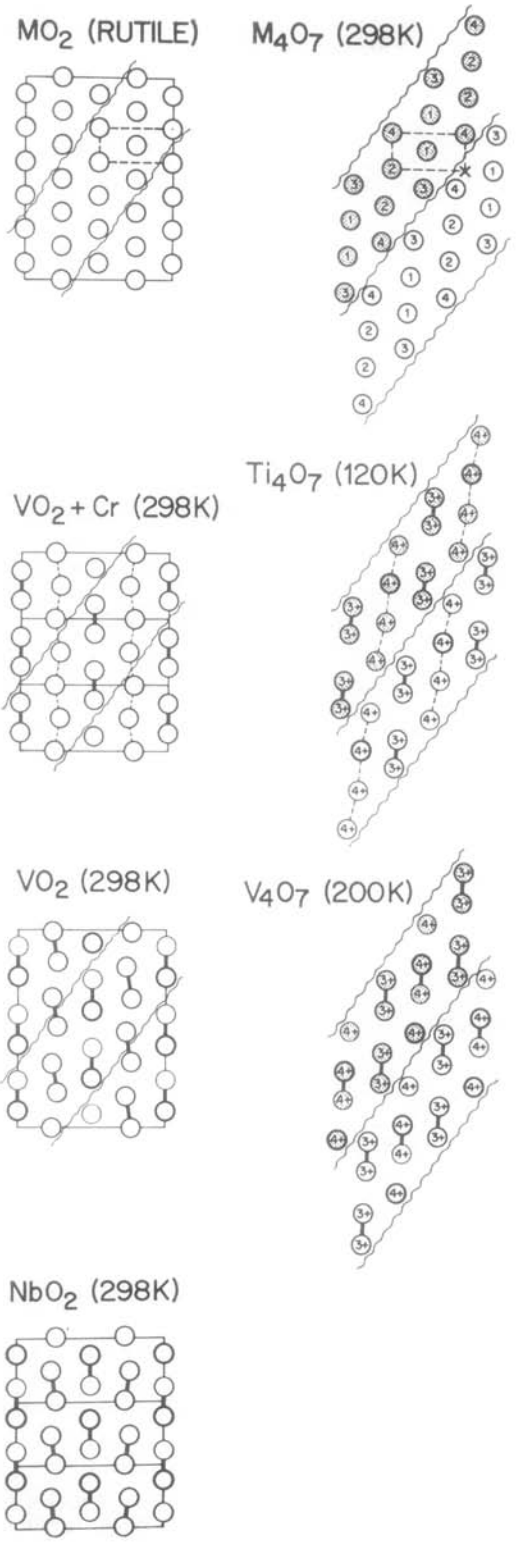

FIG. 4. Rutile and pseudorutile sections of various structures with [110] as horizontal axis and [001] as vertical axis. The wavy lines represent hypothetical and actual shear planes for the dioxides and M_4O_7 compounds, respectively. In these latter sections each pseudorutile block steps up relative to the adjacent block across the shear plane which makes an angle of approximately 65° with the plane of this page.

addition, in some of the structures the metal–metal bonds are tilted with respect to the pseudorutile *c*-axis so that the metal atoms move out of the center of the oxygen octahedra toward one oxygen. The distortions are compared in a simplified way by considering a section of the pseudorutile structure defined by the [110] and [001] rutile directions. These sections are shown in Fig. 4. There are striking similarities and differences between the bonding arrangements. In the M_4O_7 structures the rutile blocks are not wide enough to contain a complete rutile unit cell but strings of four metal atoms define the bonding pattern. There is a similarity between the pattern in pure VO_2 and that in V_4O_7 and similarly between $V_{0.976}Cr_{0.024}O_2$ and Ti_4O_7. There is no obvious geometrical reason for the structure of V_4O_7 to have some unpaired metal atoms. Hypothetical crystallographic shear planes could be drawn through the structure of monoclinic VO_2 so as to produce rutile-like blocks as in V_4O_7 but in which the cations are completely paired. Instead the shear planes run through the VO_2 structure in such a way as to cut some metal–metal bonds as illustrated in Fig. 4. In VO_2 + Cr and Ti_4O_7 half the atoms are paired and the other half form zigzag chains. In all four structures the pairs are aligned with respect to each other along the [111] pseduorutile diagonal. This is in contrast to NbO_2 where this sequence is broken.

Another common feature of all the distortions is the displacement of some of the cations out of the center of the oxygen octahedra. This results in the twisting of the bond within, or in and out of, the plane of the section shown in Fig. 4. In Ti_4O_7 and VO_2 + Cr unpaired atoms are similarly displaced. These two features (i.e., pairing and twisting) are not independent but are related by the electrostatic forces which are responsible for cohesion. Pauling's rules for the stability of complex ionic crystals state that the valence of each anion. with changed sign, is nearly equal to the sum of the electrostatic bond strengths to it from adjacent cations, i.e., $Z_{\text{anion}} = \sum_i (Z_i/\text{CN}_i) = \sum_i P_i$ where Z_i and CN_i are the charge and coordination numbers of the cations. The bond strength, P_i, is an exponential function of the metal–oxygen interatomic distance (*21*). An empirical relation can be obtained by comparing a number of different vanadium compounds with different valences and coordinations as shown in Fig. 5 (*15*, *16*, *21*, *22*). The observed V–O distances for the different oxygen

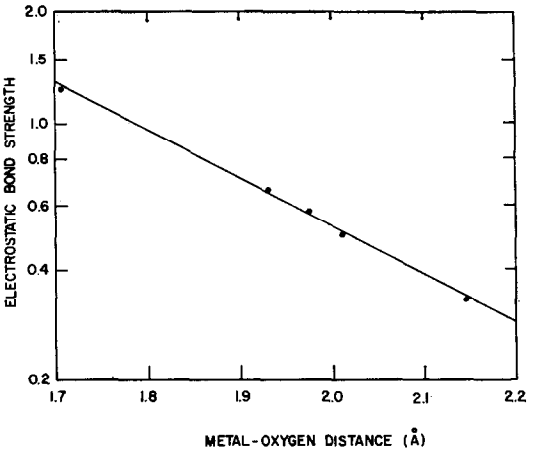

FIG. 5. Vanadium–oxygen distances vs electrostatic bond strength. Experimental points are for valence states 2^+, 3^+, 3.5^+, 4^+, and 5^+.

TABLE VII

COMPARISON OF ELECTROSTATIC BOND STRENGTHS ($\sum Z/CN$) OF OXYGEN ATOMS ABOVE AND BELOW THE METAL INSULATOR TRANSITIONS

	V_4O_7		VO_2 + Cr		VO_2	V_2O_3	
Oxygen	200K	298K	298K	360K	298K	125K	298K
1	2.09	2.07	2.00		1.95	2.01	2.04
2	2.05	2.00	2.00	1.98	2.06	2.04	
3	2.10	2.08	1.98				
4	1.84	1.85					
5	1.96	2.00					
6	1.97	2.02					
7	2.00	1.98					

atoms in each structure above and below their metal–insulator transition have been converted to bond strengths and summed. The results are shown in Table VII. It is clear that in the insulating phase of V_4O_7, V(3) moves out of the center of the octahedron toward O(3) in order to compensate the movement of V(2) and V(4) away from O(3) due to the pairing. Thus the sum of the bond strengths for O(3) are essentially identical above and below the transition. This is even clearer in VO_2 + Cr where half of the vanadium atoms pair and the other half zigzag so as to conserve electrostatic energy. In pure VO_2 all the vanadium atoms pair and twist. If the atoms only paired along the pseudorutile *c*-axis to form metal–metal bonds of equivalent length then the sums for O(1) and O(2) would be 2.31 and 1.64, respectively. By twisting, the sums are brought close to 2.00, i.e., 1.95 and 2.06. It appears that if pairing is to occur then the displacement of some of the cations must follow. On the other hand, it is not clear why in some structures only some of the atoms pair. Perhaps it is related to the fact that in all the compounds except VO_2 there is a mixture of valence states—V^{3+}, V^{4+}; Ti^{3+}, Ti^{4+}; Cr^{3+}, V^{5+}. It will be of interest to compare the bonding pattern in the phases M_nO_{2n-1} with n even with those with n odd. For the odd members, it will not be possible to have complete pairing in any chain along the pseudorutile *c*-axis.

The nature of the metal–insulator transition in V_4O_7 is markedly different from those in V_5O_9 (*23*) or Ti_4O_7 (*2*, *24*). The transitions in the latter oxides are strongly first order whereas that in V_4O_7 is only weakly first order (see Fig. 2). A similar variation with temperature has been observed in the ^{51}V NMR frequency of the 4+ sites (*25*), the resistivity (*5*), and the susceptibility (*26*). A reasonable speculation is that the atoms pair almost continuously with decreasing temperature thus causing the observed variation in the physical properties.

The problem of understanding the insulating properties of the low temperature phase of V_4O_7 is similar to that of VO_2 + Cr. Although some of the *d* electrons form nonmagnetic singlet bonds between the paired metal atoms, the *d* electrons on the unpaired metal atoms in both structures have localized. There is no observable change in symmetry or doubling of the unit cell of V_4O_7 which might produce band gaps and thus explain the insulating properties on the basis of band theory. Also, in complicated structures such as V_4O_7, it seems unreasonable to expect the *d* bands to be so narrow that small changes in lattice parameters would produce band gaps which destroy all the Fermi surface. Heat capacity and magnetic susceptibility measurements suggest that the metallic phase is highly correlated (*27*), and the X-ray evidence clearly shows charge localization in the insulating phase. It appears that in these mixed-valence oxides there is a competition between pair bonding and localization. As shown by Mössbauer (*6*) and NMR studies (*25*), V_4O_7 orders magnetically at lower temperatures and this may reflect ordering in unpaired V^{4+} cations.

Note Added in Proof. Since the writing of this paper Horiuchi et al. have published another structural refinement of V_4O_7 at room temperature. Their results agree with ours within the standard deviations. (See H. Horiuchi, M. Tokonami, N. Morimoto and K. Nagasawa, *Acta Cryst.* **B 28**, 1404 (1972).)

Acknowledgments

We thank T. M. Rice and W. F. Brinkman for helpful discussions.

References

1. M. Marezio, D. B. McWhan, P. D. Dernier, and J. P. Remeika, *Phys. Rev. Lett.* **28**, 1390 (1972).
2. M. Marezio, D. B. McWhan, P. D. Dernier, and J. P. Remeika, *J. Solid State Chem.* **6**, 419 (1973).
3. S. Andersson and L. Jahnberg, *Ark. Kemi* **21**, 413 (1963).
4. H. Horiuchi, M. Tokonomi, N. Morimoto, K. Nagasawa, Y. Bando, and T. Takada, *Mater. Res. Bull.* **6**, 833 (1971).
5. H. Okinaka, K. Nagasawa, K. Kosuge, Y. Bando, S. Kachi, and T. Takada, *J. Phys. Soc. Jap.* **28**, 798 (1970).
6. H. Okinaka, K. Kosuge, S. Kachi, M. Takano, and T. Takada, *J. Phys. Soc. Jap.* **32**, 1148 (1972).
7. K. Nagasawa, Y. Bando, and T. Takada, *Jap. J. Appl. Phys.* **8**, 1262 (1969).
8. M. Marezio, P. D. Dernier, D. B. McWhan, and J. P. Remeika, *Mater. Res. Bull.* **5**, 1015 (1970).
9. K. Nagasawa, *Mater. Res. Bull.* **6**, 853 (1971).
10. C. T. Prewitt, unpublished least-squares refinement program.
11. D. T. Cromer and J. T. Waber, *Acta. Crystallogr.* **18**, 104 (1965).
12. D. T. Cromer, *Acta Crystallogr.* **18**, 17 (1965).
13. W. R. Busing, K. O. Martin, and H. A. Levy, ORNL Report TM-306 (1964).
14. R. D. Shannon and C. T. Prewitt, *Acta Crystallogr. Sect. B.* **25**, 925 (1969).
15. J. M. Longo and P. Kierkegaard, *Acta Chem. Scand.* **24**, 420 (1970).

16. P. D. DERNIER, *J. Phys. Chem. Solids* **31**, 2569 (1970).
17. G. ANDERSSON, *Acta Chem. Scand.* **10**, 623 (1956).
18. M. MAREZIO, D. B. MCWHAN, J. P. REMEIKA, AND P. D. DERNIER, *Phys. Rev. B* **5**, 2541 (1972).
19. B.-O. MARINDER, *Ark. Kemi* **19**, 435 (1962).
20. L. PAULING, "The Nature of the Chemical Bond." Cornell University Press, Ithaca (1960).
21. H. MONTGOMERY, R. V. CHASTAIN, J. J. NATT, A. M. WITKOWSKA, AND E. C. LINGAFELTER, *Acta Crystallogr.* **22**, 775 (1967).
22. J. A. BAGLIO AND G. GASHUROV, *Acta Crystallogr. Sect. B* **24**, 292 (1968).
23. H. OKINAKA, K. NAGASAWA, K. KOSUGE, Y. BANDO, S. KACHI, AND T. TAKADA, *J. Phys. Soc. Jap.* **28**, 803 (1970).
24. R. F. BARTHOLOMEW AND D. R. FRANKL, *Phys. Rev.* **187**, 828 (1969).
25. A. C. GOSSARD AND J. P. REMEIKA, *Bull. Amer. Phys. Soc.* **17**, 959 (1972).
26. K. NAGASAWA, Y. BANDO, AND T. TAKADA, *Jap. J. Appl. Phys.* **8**, 1262 (1962).
27. D. B. MCWHAN, J. P. REMEIKA, J. P. MAITA, H. OKINAKA, K. KOSUGE, AND S. KACHI, *Phys. Rev.*, in press.